THE JOURNAL OF PHYSICAL CHEMISTRY B

Article

pubs.acs.org/JPCB

Protein Dynamics in the Solid State from ^{2}H NMR Line Shape Analysis: A Consistent Perspective

Eva Meirovitch,*[,†] Zhichun Liang,[‡] and Jack H. Freed*[,‡]

[†]The Mina and Everard Goodman Faculty of Life Sciences, Bar-Ilan University, Ramat-Gan 52900, Israel

[‡]Baker Laboratory of Chemistry and Chemical Biology, Cornell University, Ithaca, New York 14853-1301, United States

ABSTRACT: Deuterium line shape analysis of CD_3 groups has emerged as a particularly useful tool for studying microsecond−millisecond protein motions in the solid state. The models devised so far consist of several independently conceived simple jump-type motions. They are comprised of physical quantities encoded in their simplest form; improvements are only possible by adding yet another simple motion, thereby changing the model. The various treatments developed are case-specific; hence comparison among the different systems is not possible. Here we develop a new methodology for ^{2}H NMR line shape analysis free of these limitations. It is based on the microscopic-order-macroscopic-disorder (MOMD) approach. In MOMD motions are described by diffusion tensors, spatial restrictions by potentials/ordering tensors, and geometric features by relative tensor orientations. Jump-type motions are recovered in the limit of large orientational potentials. Model improvement is accomplished by monitoring the magnitude, symmetry, and orientation of the various tensors. The generality of MOMD makes possible comparison among different scenarios. CD_3 line shapes from the Chicken Villin Headpiece Subdomain and the Streptomyces Subtilisin Inhibitor are used as experimental examples. All of these spectra are reproduced by using rhombic local potentials constrained for simplicity to be given by the $L = 2$ spherical harmonics, and by axial diffusion tensors. Potential strength and rhombicity are found to be ca. 2−3 k_BT. The diffusion tensor is tilted at 120° from the C−CD_3 axis. The perpendicular (parallel) correlation times for local motion are 0.1−1.0 ms (3.3−30 μs). Activation energies in the 1.1−8.0 kcal/mol range are estimated. Future prospects include extension to the ^{2}H relaxation limit, application to the ^{15}N and ^{13}C NMR nuclei, and accounting for collective motions and anisotropic media.

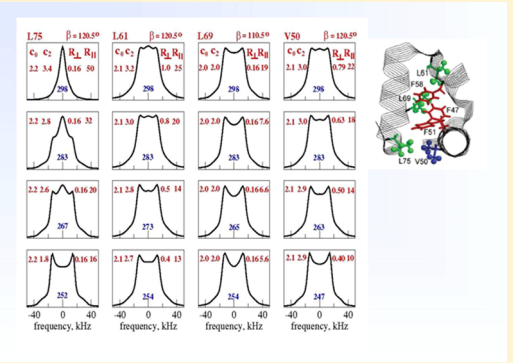

1. INTRODUCTION

Solid-state NMR spectroscopy applied to proteins is currently at the cutting edge of biostructural NMR. In parallel with advances in structure determination (e.g., ref 1 and articles cited therein) there is a surge in the development of relaxation and conformational exchange methods for characterizing internal protein mobility, using mainly ^{15}N and ^{13}C as NMR probes (e.g., refs 2−5 and articles cited therein). The relaxation limit relates to stochastic motions that are much faster than the relevant magnetic interactions. Conformational exchange is a deterministic process that relates to jumps among two or more symmetry-related sites. Together these methods cover the picosecond−millisecond range, with the protein structure mapped out effectively through uniform isotope labeling with the heteronucleus observed.

These are very attractive features. However, the experimental information consists of few parameters — T_1 and $T_{1\rho}$ for relaxation and $T_{1\rho}$ for exchange — usually acquired at a given magnetic field and temperature.[2−5] Because of the paucity of data one has to resort to severe simplifications in analyzing the experimental data. By contrast, for the ^{15}N and ^{13}C nuclei the sensitive slow-motional microsecond−millisecond range, which is amenable to investigation with NMR line shape analysis, has been explored so far qualitatively only in a few cases (e.g., ref 6).

Unlike the ^{15}N and ^{13}C nuclei, the ^{2}H nucleus bonded to sp^3-hybridized carbon emerged as a particularly useful probe over the entire dynamic range.[7−28] It has been used extensively in the relaxation limit, which applies to motions with rates exceeding approximately 10^7 s^{-1}. The typical relaxation parameters studied are ^{2}H T_{1Z} and T_{1Q}.[12,13,19,20,25] For example, methyl rotation in a small protein, investigated recently with multiple echo acquisition of T_{1Z},[19] has been interpreted in terms of jumps among three potential wells, with independent diffusive motion within the wells.[20]

The slow-motional ^{2}H range extends from approximately 10 μs to 1 ms (e.g., cf. ref 23). Line shape analyses provided insightful information on dynamic processes in hydrophobic protein cores,[17,18] membrane proteins,[29−33] collagen fibrils,[8] peptides and proteins adsorbed onto mineral surfaces,[21−24,26,27] etc. Relation to protein stability, protein folding, the assembly of collagen molecules in fibrils, the packing of secondary

Received: November 13, 2014
Revised: January 16, 2015
Published: January 16, 2015

DOI: 10.1021/jp511386b
J. Phys. Chem. B 2015, 119, 2857−2868

structure elements in globular proteins, physisorption, etc., has been established. Line shape analysis requires selective isotope labeling; effective protocols for carrying out such procedures are available.[34,35]

Deuterium NMR was used in early work to study dynamics in the solid state.[7−13,15,16] Torchia and co-workers pioneered the utilization of CD_2 and CD_3 probes to study microsecond−millisecond motions in small alanine-, methionine-, and leucine-containing peptides and collagen fibrils (e.g., refs 7 and 8). References 11, 12, 17−28, and 36−38 may be considered illustrative of the progress made since.

Theoretical developments have devised physically plausible but rather intricate and diverse models. Traditionally internal motions in proteins have been considered to be jump-type/barrier-crossing processes (e.g., ref 39). Early on it was found that a single motion of this nature does not reproduce typical experimental spectra.[40] Rather, it is necessary to combine several simple motional modes, assuming they are independent.[23,39] The key feature of asymmetry, realized in early work,[40] has been modeled in terms of unequally populated (exchange-involved) sites,[17,18,21−24] motion on arcs of variable length,[17,18,23] small-angle jumps on cones centered at tilted bond axes,[21,23] and/or motion on distorted cones.[41] Different authors conceived different combinations of simple motions. In such scenarios, where the physical quantities are encoded in their simplest form, model improvements are only possible by including in the analysis yet another simple motion, i.e., changing the overall model. Comparison among different systems featuring the same dynamic probe is not possible in view of model diversity. In some cases experimental ^{2}H line shapes could not be reproduced even with a combination of simple motions,[41] or to accomplish this, quite intricate[23] or specific[42] models had to be invoked.

No model can be proven to be unique. However, a general and comprehensive approach to the treatment of restricted motions has been developed within the scope of the Stochastic Liouville Equation (SLE) by Freed and co-workers. The SLE applies to restricted overall[43−48] as well as internal[49] motions. The major underlying factors — type of motion, spatial restrictions, and local geometry — are treated generally for the entire motional range, within their rigorous three-dimensional tensorial requirements.[43−49]

The motion *per-se* is represented by a second rank diffusion tensor, allowed to be tilted from the magnetic tensor(s). The local spatial restrictions are represented by a potential, u, expanded in the full basis set of the generalized spherical harmonics. Typically only the lowest, $L = 2$, terms are used partly for convenience, but additional terms in the expansion can be used if and when they are needed.[44,45] The $L = 2$, $K = 0$ term represents the strength of the potential; the $L = 2$, $K = 2$ term represents its rhombicity. The key element of asymmetry is thus substantiated by the (rhombic) form of the local potential. A second rank ordering tensor may be defined in terms of u. The local geometry is given by the relative orientation of the various tensors involved. Energy barriers can be realized with $L = 2$ potentials (see below). Jump-type motions can be actualized in the limit of large barriers. By including $L = 4$, $K = 0$, 2 (or higher rank/order) terms, in particular large rhombic components, in the expression for the local potential, a range of symmetries of the potential wells can be generated.[49]

The SLE described above has been used extensively for ESR applications[46,48] and in some cases for NMR applications.[14−16] Particularly relevant in the present context is the extension of the SLE called the microscopic-order-macroscopic-disorder (MOMD) approach, where the director of the local restricting environment is distributed randomly over the sample.[50] MOMD/ESR was applied to nitroxide probes in liposomes[50] and later to nitroxide-labeled proteins and DNA fragments in "frozen" solutions (i.e., scenarios where the global motion of the (typically large) molecule may be considered "frozen" on the ESR time scale).[51,52] The nitroxide label in "frozen" solutions is formally analogous to the ^{2}H label in polycrystalline proteins. *In this study we develop MOMD for the analysis of dynamic ^{2}H NMR line shapes.* Substantial changes in MOMD/ESR, associated with the ^{2}H spin Hamiltonian and the quadrupole echo excitation scheme, have been made to adapt it to ^{2}H NMR.

In MOMD one can devise analysis scenarios differing in complexity by monitoring tensor magnitude, symmetry, and orientation. This enables a continuous range of scenarios and thus comparison among different scenarios, within the scope of the same general model.

Different methyl environments within the energy landscape have been revealed.[19,20] Modification of potential energy surfaces of protein side chains by proximal surfaces has been suggested.[24] Undoubtedly, it is of interest to determine the form of the potential energy surface associated with probe dynamics. We show below potentials and associated equilibrium distribution functions emerging from MOMD/^{2}H NMR analysis. Substantial sensitivity to the symmetry of the local spatial restrictions has been detected. This is a new perspective of the local structure at methyl sites in peptides and proteins.

Vold and co-workers developed a comprehensive SLE-based computer program called EXPRESS, which treats jump-type motions in various contexts.[39] SLE-based methods for treating diffusive motions at different levels of complexity have also been developed. Thus, Wittebort and Szabo[11] treated protein side chains experiencing multiple bond rotations. The spatial constraints are accounted for by restricting the amplitudes of the internal rotations. Small-amplitude motions, associated with diffusion, were found to be ineffective in causing relaxation (of the ^{13}C label), whereas large-amplitude motions, associated with jumps, were found to be effective. On the basis of this it was concluded that jump models are appropriate. Within their scope excluded volume effects have been accounted for by considering only sterically allowed conformations. Concerted dynamics was accounted for by considering solely motions where the position of only a small number of atoms is altered.

The groups of Nordio (e.g., ref 53), Moro (e.g., ref 54), and Freed (e.g., ref 55) also developed methods for treating chain flexibility. In ref 55 torsional profiles of the chain bonds have been calculated *ab initio*. A limited number of allowed conformers that undergo torsional oscillations and conformational jumps have been identified. Similar results were obtained by Nordio, Moro, and co-workers.[53,54] Thus, more elaborate analyses have shown that chain dynamics is determined by combined diffusive and jump-type processes. Vugmeyster et al. reach similar conclusions with regard to methyl group dynamics.[20]

A method for simulating dynamic NMR spectra in rotating solids has been developed by Heaton.[56] While magic angle spinning is handled effectively, the treatment of restricted motions is rather limited. Diffusive and jump-type processes are treated alike. The motional rates are given by the elements k_{ij} of an exchange matrix and the local restrictions by $(p_i/p_j)^{1/2} \times k_{ij}$,

DOI: 10.1021/jp511386b
J. Phys. Chem. B 2015, 119, 2857−2868

where p_i and p_j are the populations of the states i and j. Typically a single rate constant is used in a given modeling procedure. Application to phenyl ring dynamics illustrates jump-type motion, whereas application to lateral diffusion across curved membranes illustrates diffusive motion.[56] This method may be considered a simple limit of MOMD.

Drobny and co-workers have studied extensively furanose ring dynamics in DNA and RNA. Their most sophisticated computer program is called KIDMAS.[42] In general, the low-energy conformations of the furanose ring cluster within two distinct energy minima identified with the pseudorotation states C2′-endo and C3′-endo. This scenario has been modeled in terms of arc-like displacements of the relevant bonds and twisting of the rings.[57] In the GCGC methyltransferase DNA recognition site the barrier between the two pseudorotation states was found to be very small. In this case furanose ring dynamics has been modeled as reorientational diffusion in a harmonic potential. Thus, Drobny et al. developed SLE-based methods featuring specific restricted diffusive motions appropriate to treat furanose ring dynamics in DNA and RNA.[42,57]

The following comment is in order. MOMD carefully considers the noncommutability of rotations. So do the programs EXPRESS[39] and KLDMAS[42]. However, the following important feature distinguishes MOMD from EXPRESS/KLDMAS. In MOMD the orientational diffusion is represented by a 3D second-rank tensor. One may use the effective 1D (isotropic diffusion tensor) version, improve the analysis by using the effective 2D (axial diffusion tensor) version, or else use the fully 3D (rhombic diffusion tensor) version. Which version is used depends on the nature of the experimental data. Likewise, the local potential may simply be described by the $L = 2$ and $K = 0$ term; this yields an axial second-rank local ordering tensor. Or, one may improve the analysis by also including the $L = 2$ and $K = 2$ term; this yields a rhombic second-rank local ordering tensor. Higher L-value and $K = 0$, $K \neq 0$ terms may also be included; this will yield higher-rank ordering tensors. Various physically relevant features of local geometry can be implemented by varying the relative orientation of the local diffusion, local ordering, and (rhombic) magnetic tensors. This is accomplished without changing the essence of the physical picture. Again, we mention that in the limit of strong orientational potentials jump-type motions of various symmetries can be implemented.

EXPRESS has been designed to treat a collection of jump-type motions. The simplest model includes a single motional mode with its specific geometric features. To improve the analysis a different motional mode with independent geometric features has to be added, etc. The essence of the physical picture (in a geometric sense and otherwise) is changed with each addition.

KLDMAS has modeled so far furanose ring dynamics within the scope of a single motional mode in terms of a one-dimensional Brownian diffuser and an axial local potential.[42] Model improvement in a geometric sense and otherwise, likely to be necessary in future work, requires generalization of this description.

MOMD can be adapted to the calculation of relaxation parameters and enhanced to include the effect of magic angle spinning.[23,25] It represents a limit of a more general two-body (protein and probe) coupled-rotator model known as the slowly relaxing local structure (SRLS) approach,[49,58,59] where the slow rotator (the protein) is so slow as to be considered rightly "frozen", yielding random orientations of the local director, i.e., MOMD. In recent years we applied the full SRLS approach to proteins in aqueous solution.[60−62] *Thus, the same general physically relevant theoretical/computational tool is now available for studying protein dynamics in the solid and liquid states.* Moreover, by implementing for protein NMR the complete SRLS theory, which also applies to the slow-motional range and to anisotropic solvents,[49] it will be possible to treat membrane proteins[29−33] which also execute slow (ms) global motion and polycrystalline proteins which execute slow (ms) collective motions[63] in addition to the currently treated localized motions.

MOMD is applicable to ^{15}N or ^{13}C line shapes. Currently few slow-motional spectra generated by these nuclei are available. A recent method, whereby internal motions are slowed down by coating the protein with trehalose without detrimental implications,[64] is expected to aid in acquiring informative slow-motional spectra.

The following comments are in order. (1) As pointed out above, MOMD and SRLS potentials can be tailored to feature potential wells.[49] Within the scope of SRLS the probe executes infrequent jumps among potential wells and fast but constrained motion within the wells.[49] This scenario is more general than just discrete jumps among wells. Currently available methods ignore mode coupling, i.e., one body moving relative to another moving body. Therefore, even if both processes are treated, statistical *independence* has to be assumed — cf. ref 20. (2) The local potential (usually defined by two coefficients), the local diffusion tensor (usually defined by two principal values and a tilt angle), and their orientational relationships to the body-fixed magnetic tensors are the only physical quantities entering the MOMD analysis. In the recent "multi-simple-mode treatments" each variable represents a different physical quantity.[18]

In this study we apply MOMD/^2H NMR to deuterated leucine and valine methyl groups of the 36-residue Chicken Villin Headpiece Subdomain (HP36)[18] and a deuterated methionine methyl group of the Streptomyces Subtilisin Inhibitor (SSI)[41]. All of these experimental spectra are reproduced with a rhombic potential and an axial diffusion tensor. We determine the strength and rhombicity of the potential for every deuterated methyl site. Typical potential forms and associated equilibrium distribution functions are illustrated. The local diffusion tensor is conveniently found to be axially symmetric and tilted from the quadrupole tensor. We determine the principal values and orientation of this tensor for every deuterated methyl site. Associated activation energies are estimated. HP36 and SSI have been analyzed previously with different multi-simple-mode models.

A brief summary of the main aspects of the Stochastic Liouville Equation underlying MOMD is presented in Section 2. Our results and their discussion appear in Section 3, and our Conclusions are summarized in Section 4.

2. THEORETICAL BACKGROUND

The theory for analyzing slow-motional magnetic resonance line shapes within the scope of the stochastic Liouville equation (SLE) is given in refs 43−46. A brief summary is presented below.

The SLE for the spin density matrix is given by

DOI: 10.1021/jp511386b
J. Phys. Chem. B 2015, 119, 2857−2868

$$\left(\frac{\partial}{\partial t}\right)\rho(\Omega, t) = [-i\mathcal{H}(\Omega)^{X} - \Gamma_{\Omega}]\rho(\Omega, t),$$
$$\text{with } \Gamma_{\Omega}P_0(\Omega) = 0 \quad (1)$$

$\mathcal{H}(\Omega)^{X}$ is the superoperator for the orientation-dependent spin Hamiltonian. Γ_{Ω} is a Markovian operator for the rotational reorientation of the spin-bearing moiety, with the Euler angles $\Omega \rightarrow (\alpha, \beta, \gamma)$ representing the orientational angles. $P_0(\Omega)$ is the unique equilibrium probability distribution of Γ_{Ω}.

A simple form of the diffusion operator, Γ_{Ω}, is[43]

$$-\Gamma_{\Omega} = R\nabla^2_{\Omega}P(\Omega, t) - (R/k_BT)(\sin\beta)^{-1}\partial/\partial\beta[\sin\beta TP(\Omega, t] \quad (2)$$

where R is the isotropic rotational diffusion coefficient, ∇^2_{Ω} is the rotational diffusion operator in the Euler angles, Ω, and T is the restoring torque. The latter is equal to $\partial u/\partial\beta$ for an axial restoring potential, e.g., $u \cong -3/2\ c_0^2\cos\beta^2$ (c_0^2 is given in units of k_BT). The general expressions for rhombic diffusion tensor, **R**, are given in ref 44. A comprehensive treatise of the SLE appears in ref 46.

In this study the probe is for convenience taken to be an axial rotator, associated in the absence of a restricting potential with three decay rates, $\tau_K^{-1} = 6R_{\perp} + K^2(R_{\parallel} - R_{\perp})$, where $K = 0, 1, 2$ (K is the order of the rank 2 diffusion tensor; $R_{\parallel}$ and $R_{\perp}$ are the principal values of **R**). One may also define $\tau_{\parallel} = 1/(6R_{\parallel})$ and $\tau_{\perp} = 1/(6R_{\perp})$.

The general form of the local potential, $u(\Omega_{CM})$, is[43]

$$u(\Omega_{CM}) = \sum_{L,K} c_K^L D_K^L(\Omega_{CM}) \quad (3)$$

C denotes the local director frame, given in this case by the equilibrium orientation of the C−CD_3 bond, and M denotes the local ordering frame (Figure 1a). If only the lowest, $L = 2$, terms are preserved (note that only even L values are considered - cf. ref 44), one obtains the rhombic potential[44,45]

$$u(\Omega_{CM}) = U(\Omega_{CM})/k_BT \approx -c_0^2D_{0,0}^2(\Omega_{CM}) - c_2^2[D_{0,2}^2(\Omega_{CM}) + D_{0,-2}^2(\Omega_{CM})] \quad (4)$$

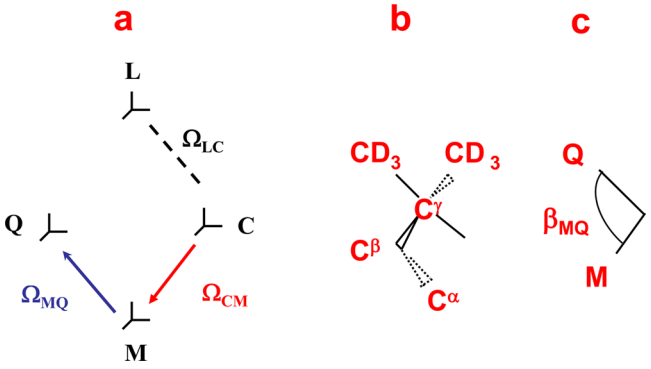

Figure 1. MOMD frames: L, lab frame; C, local director frame; M, local ordering/local diffusion frame; Q, frame/principal axis of (axial) quadrupole tensor $\langle\mathbf{Q}\rangle$ (a). Stereochemical context for (leucine) C^{γ}−CD_3 motion (b). MOMD axes associated with C^{γ}−CD_3 motion: Q, principal axis of $\langle\mathbf{Q}\rangle$; M, principal ordering/diffusion axis. Here $\beta_{MQ} = 110.5°$ (corresponding to motion around the C^{β}−C^{γ} bond for sp^3-hybridized carbon atoms) (c).

The coefficient c_0^2 evaluates the strength of $u(\Omega_{CM})$, and c_2^2 evaluates its nonaxiality (both in units of k_BT).

Local order parameters are defined as[44,45]

$$\langle D_{0,K}^2(\Omega_{CM})\rangle = \int d\Omega_{CM} D_{0,K}^2(\Omega_{CM})\exp[-u(\Omega_{CM})]/\int d\Omega_{CM}\exp[-u(\Omega_{CM})], \quad K = 0, 2 \quad (5)$$

For at least 3-fold symmetry around Z_C, the Z axis of the local director frame, and at least 2-fold symmetry around Z_M, the principal axis of the local ordering tensor, only $S_0^2 \equiv \langle D_{0,0}^2(\Omega_{CM})\rangle$ and $S_2^2 \equiv \langle D_{0,2}^2(\Omega_{CM}) + D_{0,-2}^2(\Omega_{CM})\rangle$ survive.[44] The Saupe scheme order parameters relate to S_0^2 and S_2^2 as $S_{xx} = ((3/2)^{1/2}S_2^2 - S_0^2)/2$, $S_{yy} = -((3/2)^{1/2}S_2^2 - S_0^2)/2$, and $S_{zz} = S_0^2$.

Figure 1a shows the MOMD frame structure for C−CD_3 bond dynamics. L denotes the laboratory frame. C (local director frame) and M (local ordering/local diffusion frame taken as coincident for simplicity) have been defined above. Q denotes the principal axis system (PAS) of the effective quadrupole tensor, $\langle\mathbf{Q}\rangle$. The Euler angles Ω_{CM} are time-dependent. The Euler angles Ω_{MQ} are time-independent. Since there is no "macroscopic order", one has to calculate ^{2}H spectra for every Ω_{LC} and convolute the corresponding line shapes according to a random distribution.[50]

3. RESULTS AND DISCUSSION

3.1. Model. Fast methyl rotation in the C−CD_3 moiety reduces the C−D quadrupole constant from 167 kHz (e.g., ref 60) to $167 \times [1.5\ \cos^2(110.5°) - 0.5] = 52.8$ kHz (the tetrahedral angle of 110.5° corresponds to sp^3-hybridized carbon). Figure 1b shows the leucine side-chain stereochemistry. In the multi-simple-mode paradigm each component is consistent with a specific feature of Figure 1b. The model used to treat C−CD_3 dynamics in HP36 (ref 18) combines (1) fast methyl rotation accounted for by a partially averaged quadrupole constant of 53.3 kHz; (2) restricted diffusion of the methyl axis on an arc approximated by small nearest-neighbor jumps; and (3) rotameric interconversion corresponding to jumps between four out of the nine nonequivalent configurations of the leucine side chain. The parameters varied include the length of the arc, the jump rate on the arc, the rate of the rotameric jumps, and the populations of the sites among which the rotameric jumps occur (one major conformer and three equally populated minor conformers). The quadrupolar frame, Q, of the $\langle\mathbf{Q}\rangle$ tensor is implicitly parallel to the C^{γ}−C^{δ} bond.

MOMD treats C^{γ}−CD_3 leucine dynamics with a conceptually simple mesoscopic tensorial approach. A single model-related frame, M, a single NMR-related frame, Q, and their relative orientation (β_{MQ}), are featured (Figure 1c). Relation to Figure 1b is implicit in the values of the MOMD parameters. *Based on this frame structure underlying the theory presented in section 2, we have developed a theoretical/computational tool for analyzing ^{2}H NMR lineshapes from polycrystalline proteins.* The parameters varied include, in general, the strength and rhombicity of the local potential, u (c_0^2 and c_2^2 in eq 4), the principal values of the local diffusion tensor, **R** ($R_{\parallel}$ and $R_{\perp}$), and the relative orientation of the local ordering/local diffusion and quadrupolar tensors (β_{MQ}).

3.2. Key Parameters: Sensitivity and Versatility. The time-range amenable to investigation is determined by the partially averaged quadrupole constant, $\langle Q\rangle$. The inverse of $\langle Q\rangle$ (more generally, of a given magnetic interaction, Δ) in

DOI: 10.1021/jp511386b
J. Phys. Chem. B 2015, 119, 2857−2868

appropriate units is a typical correlation time, $\tau_{\langle Q \rangle}$, yielding a dynamic line shape. For $\langle Q \rangle$ = 52.8 kHz one has $\tau_{\langle Q \rangle}$ = 0.11 ms.

3.2.1. Simple Parameter Combination. Axial local potential, isotropic local diffusion, and collinear local ordering/local diffusion and quadrupolar frames constitute the simplest parameter combination. We check whether this scenario reproduces the main features of the ^{2}H line shapes from HP36 (depicted as a ribbon diagram in Figure 2). The

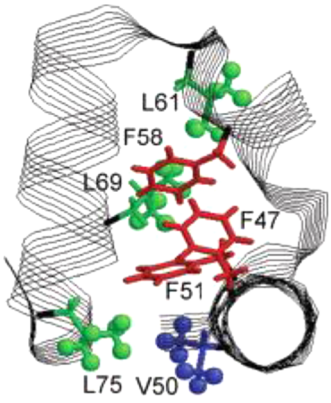

Figure 2. Ribbon diagram of the protein HP36, with the selectively deuterated methyl groups depicted.

temperature-dependent ^{2}H spectra from one of the two methyl groups of the leucine residues L75, L61, and L69 and the methyl groups of the valine residue V50 are represented by the red traces in Figure 3 (taken from ref 18).

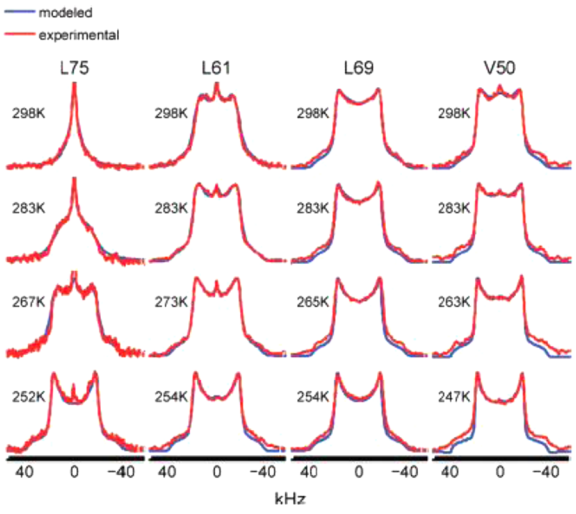

Figure 3. Experimental (red) and modeled in ref 18 (blue) ^{2}H line shapes obtained from the selectively deuterated methyl groups L75, L61, L69, and V50 of HP36.

The potential coefficient, c_0^2, was varied in the 1−15 range, while the correlation time for local diffusion, $\tau = 1/(6R)$, was varied in the 1 μs−5 ms range; the angle β_{MQ} was set equal to zero. Qualitative agreement with the low-temperature spectra in Figure 3 was achieved with $\langle Q \rangle$ = 52.8 kHz, an intrinsic line width, $(T_2^*)^{-1}$, of 1 kHz, c_0^2 on the order of 2 (in units of k_BT), and local motional correlation times of 1−2 ms. Weak local potentials are consistent with previous SRLS analyses of methyl dynamics in protein dissolved in aqueous solution.[65] They are also consistent with relatively small squared generalized order parameters of methyl groups attached to long side chains of proteins in solution.[66] Figure 4a shows ^{2}H MOMD spectra

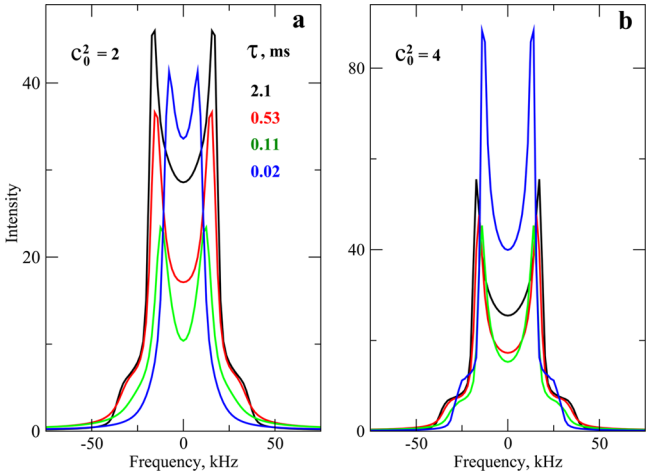

Figure 4. ^{2}H MOMD line shapes calculated using $c_0^2 = 2$ (a) and $c_0^2 = 4$ (b), motional correlation times as depicted, and β_{MQ} = 110.5°. Additional parameters used include $\langle Q \rangle$ = 52.8 kHz and an intrinsic line width, $(T_2^*)^{-1}$, of 1 kHz.

scanning the entire dynamic range, which for c_0^2 = 2 extends from $\tau \sim 2$ ms (rigid-limit) to $\tau \sim 20$ μs (extreme motional narrowing limit). In Figure 4b we show analogous line shapes obtained for c_0^2 = 4. The agreement with the low-temperature spectra of Figure 3 is worse for c_0^2 = 4 as compared to c_0^2 = 2.

The c_0^2 = 2 spectra (Figure 4a) are quite sensitive to τ both in the "shoulder" region (corresponding to the parallel orientation) and in the "horn" region (corresponding to the perpendicular orientation). The sensitivity of the analysis to parameter variations is substantially more limited for c_0^2 = 4 (Figure 4b). In both cases the central "depression" decreases in intensity with decreasing τ for $\tau > \tau_{\langle Q \rangle}$, while the opposite trend is observed for $\tau < \tau_{\langle Q \rangle}$. The overall spectral width decreases as the local motion becomes faster for both c_0^2 = 2 and c_0^2 = 4. The experimental spectra of L69 have a decreasing central depression with increasing temperature and a largely temperature-invariant overall width, in disagreement with Figure 4. Thus, an important factor appears to be missing in these simulations, which do not reproduce even the relatively simple line shape evolution of L69.

A straightforward improvement is to allow the angle β_{MQ} to vary. Since the local ordering tensor is axially symmetric, the angle β_{MQ} between the principal axes of the M and Q frames should affect the predicted spectrum. We found that within the scope of isotropic local diffusion the effect of β_{MQ} being different from zero is small. The multi-simple-mode approaches feature scalar parameters (formally analogous to the rate or correlation time for isotropic diffusion in MOMD) as descriptors of the local motions. That a single motional mode of this nature cannot reproduce experimental ^{2}H line shapes with characteristic geometric features is consistent with the finding delineated above. That appropriate tensorial description actualizes a single generally applicable motional mode is shown in the forthcoming.

3.2.2. Axial Potentials and Axial Diffusion. We proceed by allowing for axial local diffusion. To test sensitivity we set c_0^2 = 2, $\tau_\perp$ equal to $\tau_{\langle Q \rangle}$ = 0.11 ms, and vary $\tau_\parallel$ as shown in Figure 5

DOI: 10.1021/jp511386b
J. Phys. Chem. B 2015, 119, 2857−2868

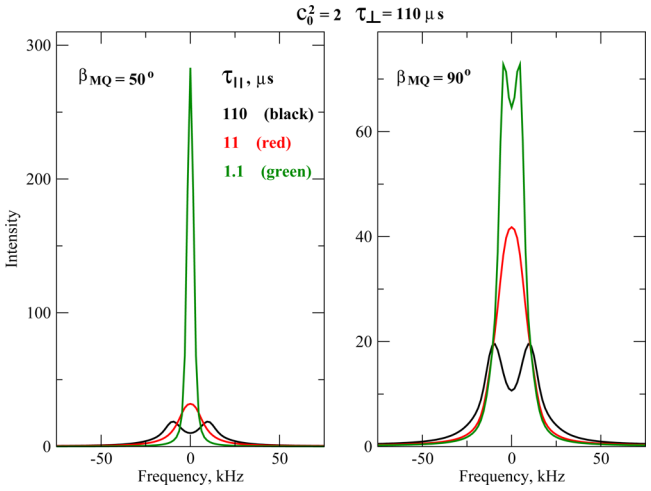

Figure 5. MOMD ^{2}H line shapes for β_{MQ} = 50° (a), 90° (b), and local motional correlation times as depicted. Additional parameters used include ⟨Q⟩ = 52.8 kHz and $(T_2^*)^{-1}$ = 1 kHz.

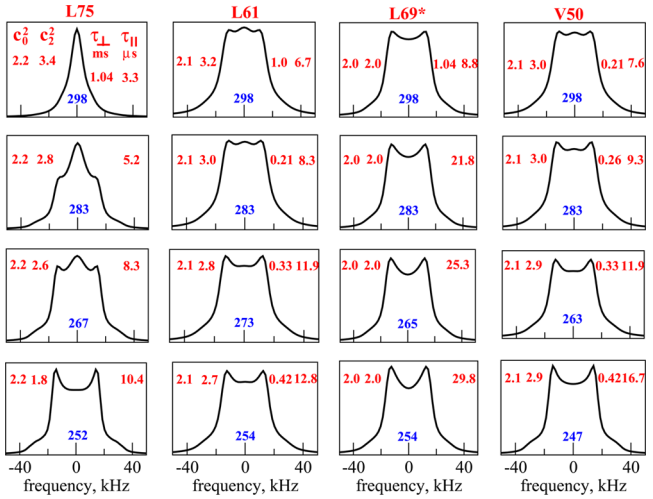

Figure 6. ^{2}H MOMD line shapes calculated for rhombic potentials with c_0^2 and c_2^2 as depicted, axial local diffusion with $\tau_{||}$ and $\tau_\perp$ as depicted, and tilt angle β_{MQ} = 120° (except for L69 — denoted with an asterisk — where β_{MQ} = 110.5°).

for β_{MQ} = 50° and 90° (note that in a mesoscopic approach preferential ordering does not have to — although it certainly may — point along a chemical bond). It can be seen that corresponding line shapes in parts (a) and (b) differ to a very large extent, bearing out the substantially enhanced sensitivity of the analysis to the local geometry within the scope of axial diffusion.

Although we allowed c_0^2, β_{MQ}, $\tau_\perp$, and $\tau_{||}$ to vary freely, the line shape *evolutions* depicted in Figure 3 have not been reproduced satisfactorily by our MOMD calculations. We conclude that an important factor is still missing in our simulations.

3.2.3. Rhombic Potentials. A key feature that emerged from our previous SRLS-based studies of NMR relaxation in aqueous protein solutions,[61,62,65,67,68] and from previous studies of ^{2}H line shapes in polycrystalline peptides and proteins[17−27,41] is the need to account for the asymmetry of the local spatial restrictions. Within the scope of MOMD this property is expressed in terms of rhombic local potentials/local ordering. We find that the main features of Figure 3 line shapes are reproduced with rhombic potentials with c_0^2 and c_2^2 on the order of 2−3. Our best-fit line shapes (based on visual comparison) are shown in Figure 6, together with the respective best-fit parameters. For easy comparison with their experimental counterparts shown in Figure 3, we also specify the temperatures in blue (Figure 6).

Detailed discussion of our results appears below. Note that we do not impose Arrhenius-type temperature dependence on the motional rates. However, we do not accept results where the temperature-dependent line shape evolution yields rates that vary in an unphysical manner.

3.3. MOMD Applied to the Chicken Villin Headpiece Subdomain. All of the calculations presented below used ⟨Q⟩ = 52.8 kHz and an intrinsic line width of 1 kHz. Initially the angle β_{MQ} was set equal to 110.5°. For leucine (valine) residues this is consistent with two-site exchange around the $C^\beta-C^\gamma$ ($C^\alpha-C^\beta$) bond (e.g., ref 8). Except for the rather insensitive L69 line shapes, the spectra shown in Figure 3 could not be reproduced satisfactorily with β_{MQ} = 110.5°. On the other hand, $\beta_{MQ} \cong 120°$ yielded satisfactory results.

The description of the local geometry in previous studies is very diverse. The angle between exchanging C−D or $C-CD_3$ bonds, considered as the main dynamic mode, was ascribed quite different values in different multimode analyses. It was determined as 108°−112° in ref 8, 32°−90° in ref 28, 90° in ref 7, 60°−80° in ref 41, 120° in ref 36, etc. As indicated above, these are effective angles. It is of interest, though, that the value of 120° determined by our MOMD analysis is the angular minimum for trans−gauche isomerization.[36] We estimate the error in β_{MQ} as ±3°.

With β_{MQ} fixed at 120°, we proceeded varying c_0^2, c_2^2, $\tau_\perp = 1/(6R_\perp)$, and $\tau_{||} = 1/(6R_{||})$.

The line shapes of L69 vary to a relatively small extent. The nearly constant overall width and the slight reduction in the central depression with increasing temperature have been reproduced with rhombic potential given by c_0^2 = 2.0 and c_2^2 = 2.0. The lower limit of $\tau_\perp$, which is too slow to affect the analysis, has been set at 1.04 ms. $\tau_{||}$ ranges from 29.8 μs at 254 K to 8.8 μs at 298 K, with an activation energy of E_a = 8.0 kcal/mol. The latter is substantially larger than the activation energies associated with all of the other methyl groups investigated (see below). This is consistent with L69 being effectively secluded in the protein core. Indeed, unlike all of the other deuterated methyl groups of HP36, the deuterated methyl group of L69 yields at 298 K virtually identical spectra in hydrated and dry polycrystalline powder samples.[18] By contrast, the authors of ref 18 found that the activation energy for L69 is the smallest among all of the activation energies determined.

The errors in c_0^2, c_2^2, $\tau_\perp$, and $\tau_{||}$ are estimated at 10%. The errors in the activation energies associated with $R_\perp$ and $R_{||}$ given below are estimated at 15%. These evaluations apply to all of the MOMD calculations shown and discussed below.

The line shapes of V50 feature a cusp at zero frequency at, and above, 263 K. The authors of ref 23 pointed out difficulties in reproducing this feature. As shown below, MOMD reproduces it satisfactorily. The temperature-dependent line shapes of V50 can be reproduced with a potential strength given by c_0^2 = 2.1, rhombicity increasing slightly from c_2^2 = 2.9 at 247 K to c_2^2 = 3.0 at 298 K, and a decrease in $\tau_\perp$ ($\tau_{||}$) from 0.42 ms (16.7 μs) at 247 K to 0.21 ms (7.6 μs) at 298 K. The activation energies are 1.9 kcal/mol for $\tau_\perp$ and 2.3 kcal/mol for $\tau_{||}$.

DOI: 10.1021/jp511386b
J. Phys. Chem. B 2015, 119, 2857−2868

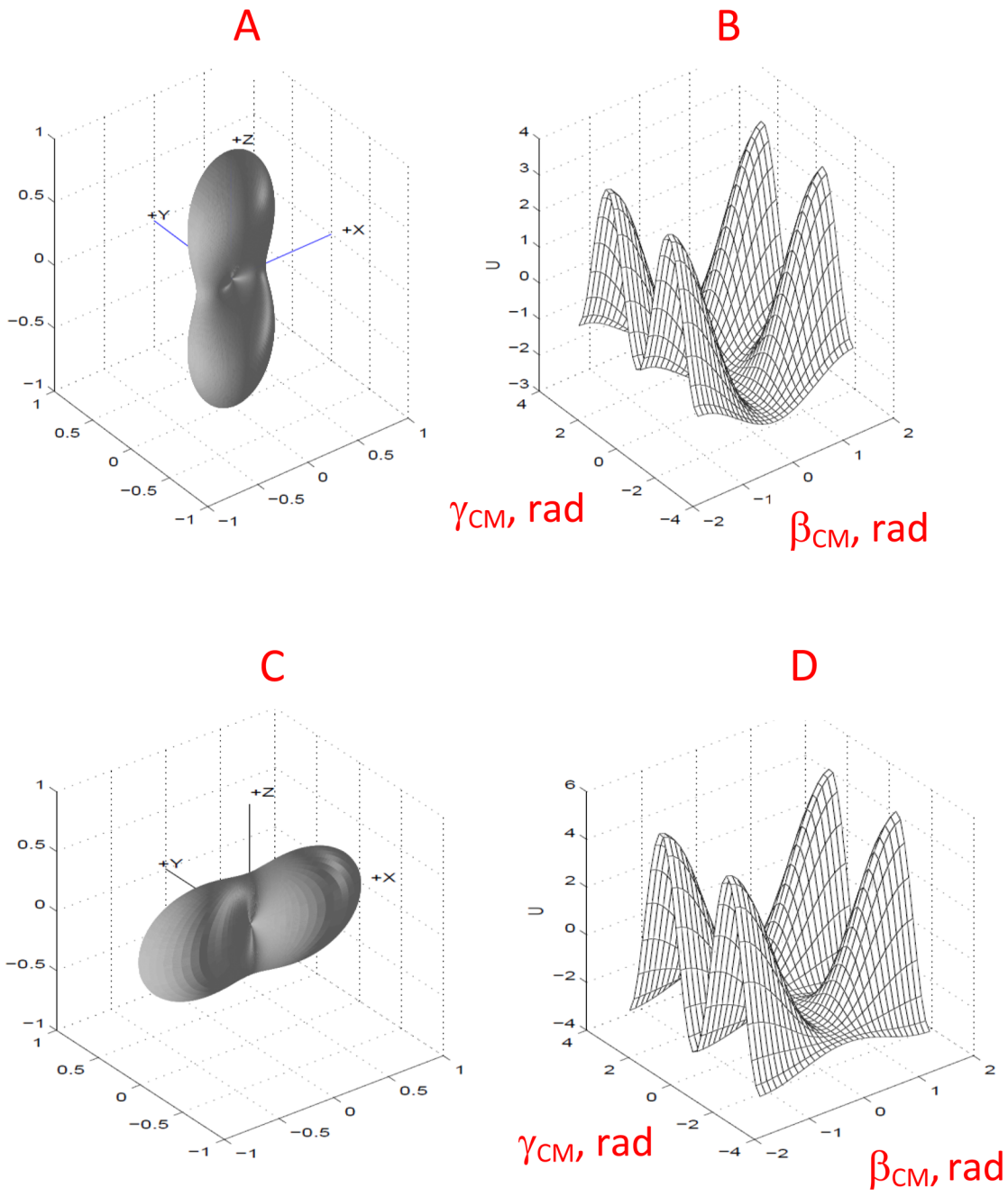

Figure 7. Equilibrium probability distribution function, $P_{eq}(\beta_{CM},\gamma_{CM})$, depicted as $X_C = R\sin(\beta_{CM})\cos(\gamma_{CM})$, $Y_C = R\sin(\beta_{CM})\sin(\gamma_{CM})$, and $Z_C = R\cos(\beta_{CM})$, where $R = \exp(-u)$ (part **A**), corresponding to the MOMD potential, $u(\beta_{CM},\gamma_{CM})$, given by $c_0^2 = 2.2$ and $c_2^2 = 1.8$ (part **B**). Equilibrium probability distribution function, $P_{eq}(\beta_{CM},\gamma_{CM})$ (part **C**), corresponding to the MOMD potential, $u(\beta_{CM},\gamma_{CM})$, given by $c_0^2 = 2.2$ and $c_2^2 = 3.4$ (part **D**).

The L61 line shape evolution with temperature has been reproduced with $c_0^2 = 2.1$ and c_2^2 increasing from 2.7 at 254 K to 3.2 at 298 K. $\tau_\perp$ changes from 0.42 ms at 254 K to 1.0 ms at 298 K with an activation energy of 3.3 kcal/mol. $\tau_\parallel$ changes from 12.8 ms at 254 K to 6.7 ms at 298 with an activation energy of 2.5 kcal/mol. The differences between corresponding parameters of V50 and L61 are relatively small, except for the activation energies, which are substantially larger for L61. This is likely to be due to factors associated with methyl-type and/or residue location (V50 is located in helix 1 and L61 at the interface of helix 2 and the loop connecting helices 2 and 1).

The line shapes of L75 exhibit the largest variation as a function of temperature. The rhombicity of the local potential increases substantially from $c_2^2 = 1.8$ at 252 K to 3.4 at 298 K. The correlation time $\tau_\perp$ is too slow to affect the analysis. The correlation time $\tau_\parallel$ (10.4 μs at 252 K and 3.3 μs at 298 K) is associated with the very small activation energy of 1.1 kcal/mol (in ref 18 L75 is associated with very large activation energy). That smaller energy barriers have to be surmounted in the unstructured C-terminal segment housing L75, as compared to secondary-structure elements housing L61, L69, and V50, is expected.

For all of the methyl groups studied except for L69 we find that the rhombicity of the local potential *increases* with increasing temperature. At first glance this is rather surprising. However, if two (or more) different sources of temperature-dependent structural changes are contributing to this potential, it would not be surprising. For example, the local ordering

DOI: 10.1021/jp511386b
J. Phys. Chem. B 2015, 119, 2857−2868

tensors (defined in terms of the respective potentials) associated with these sources could be mostly axial but tilted with respect to each other. When both sources are operative, say at higher temperatures, the effective potential becomes rhombic. When one nearly freezes out at lower temperatures, the rhombicity of the effective potential becomes reduced substantially.

We associate the persistent source with proximal restraints and the source prone to freeze out at lower temperatures with distal restraints. For HP36 the latter play a particularly important role in stabilizing the tertiary structure in view of the exceptionally small area/volume ratio of this protein, which renders the sequestering of the hydrophobic residues more difficult.

In this context we show in Figure 7 local potentials, $u(\beta_{CM},\gamma_{CM})$, and the associated equilibrium probability distribution functions, $P_{eq}(\beta_{CM},\gamma_{CM})$. The latter are depicted as $X_C = R\sin(\beta_{CM})\cos(\gamma_{CM})$, $Y_C = R\sin(\beta_{CM})\sin(\gamma_{CM})$, and $Z_C = R\cos(\beta_{CM})$, where $R = \exp(-u)$. We show data for L75 at 252 K, where $c_0^2 = 2.2$ and $c_2^2 = 1.8$, and at 298 K, where $c_0^2 = 2.2$ and $c_2^2 = 3.4$. At 252 K preferential ordering occurs along Z_C, indicating parallel ordering. This corresponds to a nearly axial/slightly rhombic scenario, in agreement with the distal restrains being nearly frozen. At 298 K preferential ordering occurs along X_C, indicating perpendicular ordering. We analyzed previously with SRLS ^{2}H relaxation from methyl groups in proteins dissolved in aqueous solution. In many cases the rhombicity of the local potential was found to be very large and the tilt between the main ordering axis and the principal axis of the $\langle \mathbf{Q} \rangle$ tensor nearly 110.5°. X_C ordering is consistent with this geometric scenario.

An interesting future prospect is to correlate the mesoscopic local potentials and associated equilibrium distribution functions obtained with MOMD with their atomistic counterparts calculated with molecular dynamics (MD) simulations.

Figure 8A shows experimental spectra from the surface-exposed residue L63 (left) and a free peptide comprising helix h3 of HP36, labeled at the position of L69 (right). Figure 8B (or Figure 9) shows the respective best-fit MOMD line shapes. Corresponding parameters are quite similar, except for the significant increase in potential rhombicity with increasing temperature for L63 as compared to constant rhombicity for L69 in the free peptide. This can be rationalized as follows. For L63 the tilt between the proximal/distal ordering frames is virtually independent of temperature. For the free peptide it changes with temperature such that the effective potential becomes more rhombic at higher temperatures.

Figure 10 shows MOMD spectra for L69 in the protein core and L69 in the free peptide at similar temperatures. In the spirit of the interpretation delineated in the preceding paragraph (cf. Figures 9 and 10), the relative orientation of the proximal/distal ordering frames differs in these two scenarios such that the rhombicity of the effective potential is larger in the free peptide.

Proximal/Distal Restraint Proposal. Several independent studies of HP36 have provided information related to our proximal/distal restraint proposal. A brief summary of the findings relevant to the matter in point follows.

A large number of studies associated with HP36 focus on the folding aspect. The consensus, based primarily on molecular dynamics (MD) simulations, appears to be fast consolidation of the secondary structure and much slower consolidation of the tertiary structure. This may be associated with difficulty in the formation of distal restraints. Temperature-dependent backbone dynamics of HP36 in solution was studied previously using model-free as a method of analysis.[69] The key parameter derived is the squared generalized order parameter, S^2. The results indicate that the temperature dependence of S is not described accurately by axial model potential functions for bond vector reorientation used previously in this context for larger proteins. This is consistent with the rhombic local potentials determined in the solid state by the MOMD analysis.

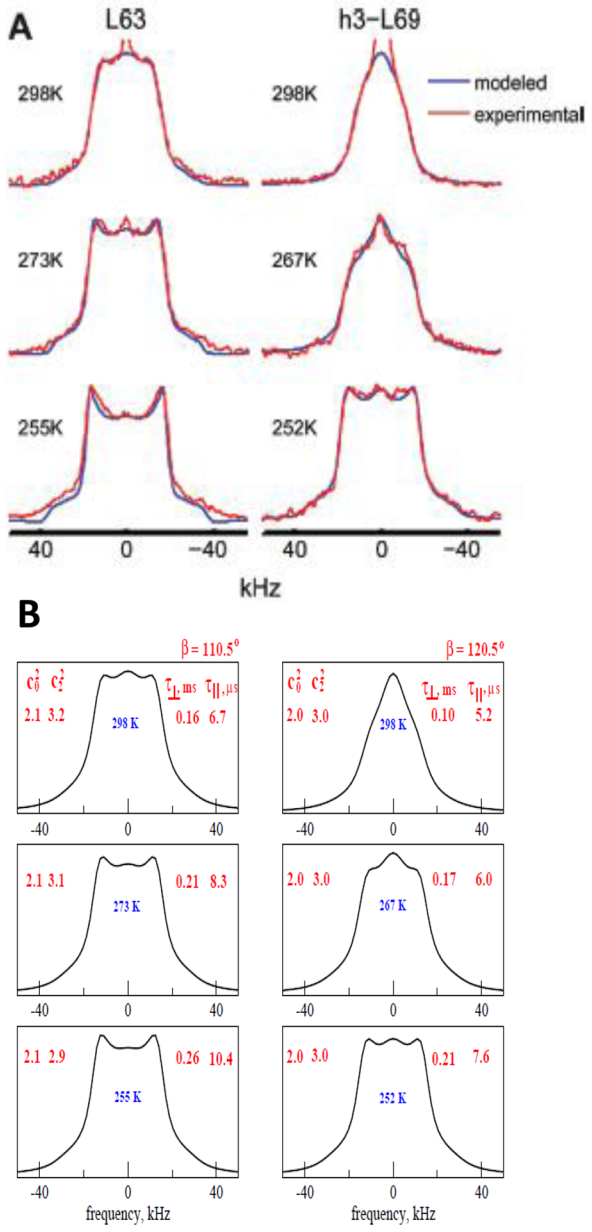

Figure 8. Experimental (red) and modeled in ref 18 (blue) ^{2}H line shapes from the deuterium-labeled methyl group of the surface residue L63 and the h3-L69 peptide (A). Same as the captions of Figure 9(B).

Several published studied make possible a more direct comparison of their results with the proximal/distal restraint concept. For example, Herges and Wenzel[70] investigated the free-energy landscape of HP36 and the 40-residue HIV Accessory Protein (HAP) with molecular dynamics (MD) simulations. While HAP exhibits a distinct global minimum, HP36 exhibits quite a few metastable states with free energy comparable to that of the global minimum. Reaching the global

DOI: 10.1021/jp511386b
J. Phys. Chem. B 2015, 119, 2857−2868

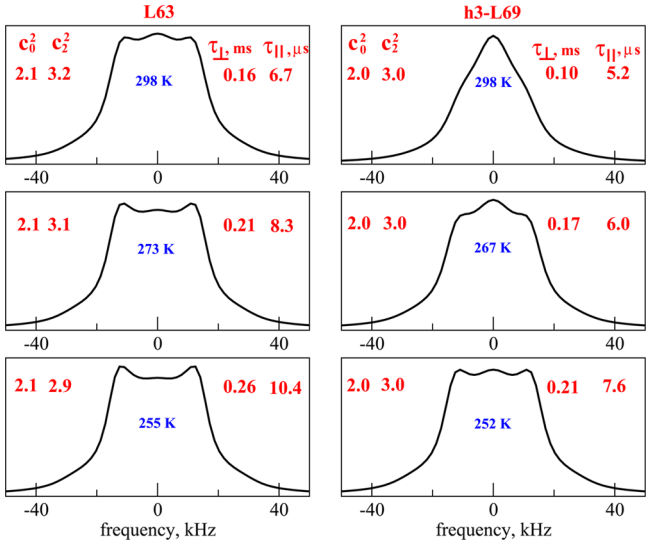

Figure 9. Best-fit MOMD line shapes for the experimental spectra shown in Figure 8A, calculated using $\langle Q \rangle$ = 52.8 kHz, $(T_2^*)^{-1}$ = 1 kHz, β_{MQ} = 120°, and the parameters depicted on the figure.

minimum took ten times longer for HP36 as compared to HAP. These observations are consistent with the very small protein HP36, unlike the common protein HAP, requiring extra global-minimum-stabilizing distal restraints to fold properly.

Usually X-ray crystallography and NMR structures of single-domain proteins do not differ considerably. In the case of HP36, substantial differences have been detected.[71] To reveal their origin, MD simulations were carried out starting with the NMR structure. After 50 ns HP36 spontaneously adopted conformations more consistent with the crystal structure. Unlike the solution structure, these conformations featured a stable distance between F47 and R55, suggesting the formation of a cation−π interaction. Experimental double mutant cycles confirmed that the F47−R55 pair has a relatively large energetic coupling. In light of these observations the authors of ref 71 consider the X-ray crystal structure an appropriate representation of HP36 in solution at neutral pH.

This may be rationalized as follows. The interaction between F47 and R55 is a distal restraint in the global minimum crystal structure. It is not stable in the solution structure which is an average comprising among others the global minimum. Recovering the latter requires extensive conformational search.

A recent study reported on the response of HP36-coated gold nanoparticles (AuNPs) to ultrafast laser heating.[72] Laser pulse radiation for maximal heating altered substantially the structure of proteins used previously as AuNP-coating agents. Surprisingly, it left intact the 3D structure of HP36. This may be rationalized as follows. In the coating layer the HP36 molecule is flanked by thiolated polyethylene glycol (briefly PEG). The potentially available distal interactions are utilized by PEG to stabilize the structure of HP36 in the coating layer. Such potential interactions are not available in other proteins.

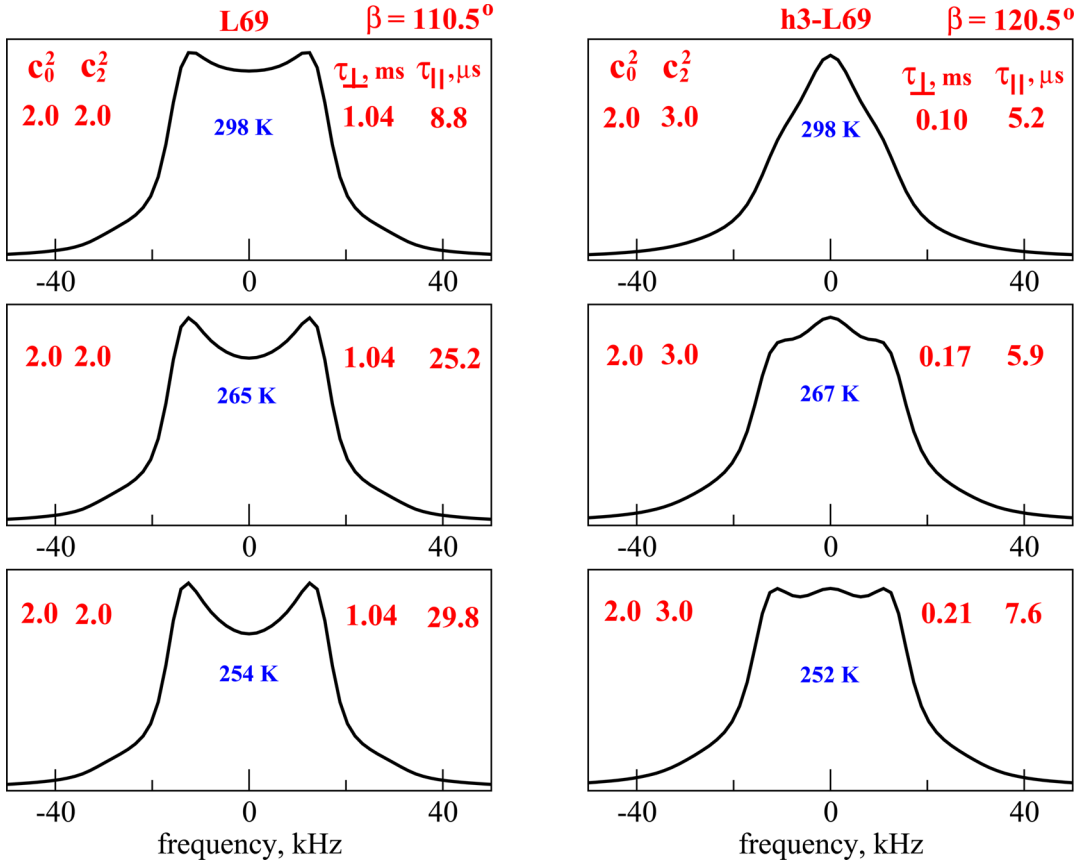

Figure 10. Best-fit MOMD ^{2}H spectra of L69 for 254, 265, and 298 K (experimental spectra shown in Figure 3), and best-fit MOMD spectra of the h3-L69 peptide for 252, 267, and 298 K (experimental spectra shown in Figure 8A). The MOMD calculations were carried out using $\langle Q \rangle$ = 52.8 kHz, $(T_2^*)^{-1}$ = 1 kHz, β_{MQ} = 120°, and the parameters depicted on the figure.

DOI: 10.1021/jp511386b
J. Phys. Chem. B 2015, 119, 2857−2868

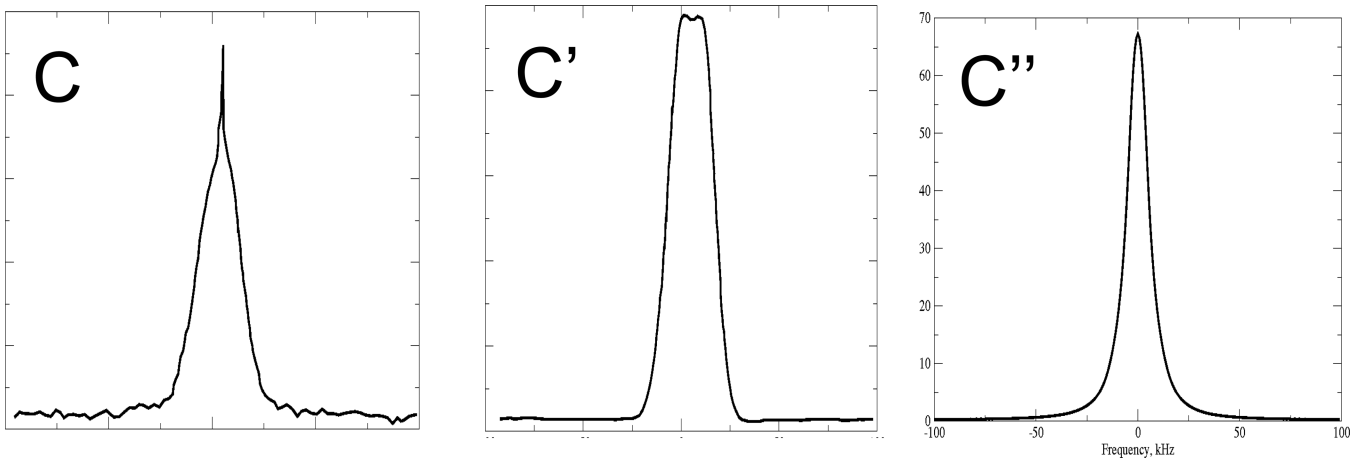

Figure 11. Experimental ^{2}H line shape from the selectively deuterated methyl group of Met 73 of the Streptomyces Subtilisin inhibitor (C). Corresponding best-fit spectrum obtained in ref 41 (C′). MOMD spectrum obtained for $\langle Q \rangle$ = 52.8 kHz, $(T_2^*)^{-1}$ = 1 kHz, β_{MQ} = 120°, c_0^2 = 2.2, c_2^2 = 1.6, $\tau_\perp$ = 1.04 ms, and $\tau_\parallel$ = 3.3 μs (C″).

Thus, independent studies provide information consistent with our proximal/distal restraint proposal.

Comparison with the Multi-Simple-Mode Analysis of HP36. The authors of ref 18 specify the room-temperature (298 K) rates for L75 and L69. The values are 1.04×10^4 s^{-1} (given as 6.5×10^4 rad/s in the article) for L75 and 0.37×10^4 s^{-1} (given as 2.3×10^4 rad/s) for L69. The analogous MOMD data are 5.05×10^4 s^{-1} (3.3 μs) for L75 and 1.9×10^4 s^{-1} (8.8 μs) for L69. The MOMD rate constants are five times faster than the rate constants for the dominant motional mode of the multi-simple-mode scenario. In comparing them one must appreciate that the effective MOMD rates also include the effect of the potential barriers, which slow down the diffusive motion.[49]

3.4. MOMD Applied to the Streptomyces Subtilisin Inhibitor. This protein has been ^{2}H-labeled selectively at the methyl groups of residues Met 103, Met 73, and Met 70.[41] Here S−CD_3 dynamics is investigated. ^{2}H line shapes were acquired from polycrystalline samples of the respective mutants as a function of hydration. Simulations based on discrete jumps around axes tilted from the S−CD_3 bond to various extents, and among sites with various relative populations, were carried out. Some spectra were reproduced satisfactorily. Several important spectra could not be reproduced following this approach. Figure 11C shows such a spectrum obtained from the methyl group of Met 73 in a sample containing 0.6 g of H_2O per g of protein−water. This scenario is typical of the native protein in the solid state;[41] hence, it is particularly important.

The Figure 11C spectrum features dominant intensity at zero frequency (ignoring the spike associated with residual HDO) and gradual descent to the baseline. Figure 11C′ shows the best-fit spectrum which the authors of ref 41 could obtain. The model used consists of random jumps among four equally populated sites on a distorted cone, with a rate of 10 MHz, 0.5 kHz Lorentzian line broadening, and 10 kHz Gaussian line broadening. The shape of the spectrum around zero frequency, which is a dominant feature, has not been reproduced properly.

Figure 11C″ shows the MOMD line shape obtained for a rhombic local potential with c_0^2 = 2.2, c_2^2 = 1.6, $\tau_\perp$ = 1.04 ms, $\tau_\parallel$ = 3.3 μs, and β_{MQ} = 120°. The agreement with the experimental spectrum of Figure 11C has been improved substantially. At least in this case, MOMD-based analysis yields better agreement than the multisimply mode approach.

4. CONCLUSIONS

The MOMD approach interprets the main features of ^{2}H line shapes representing microsecond−millisecond C−CD_3 and S−CD_3 bond dynamics in proteins in terms of a single (effective) dynamic mode. The latter features a local potential and a local diffusion tensor as qualifiers of structural dynamics. The local potential is typically rhombic; its strength and deviation from axiality are approximately 2 k_BT. The local diffusion tensor may be taken as axially symmetric, with principal axis tilted at 120° (the angular minimum for trans−gauche isomerization) from the C−CD_3 bond. The perpendicular (to the principal axis of the diffusion tensor) correlation time is in the 0.1−1.0 ms range. The parallel correlation time is in the 3.3−30 μs range. The analysis leads to Arrhenius temperature behavior with respective activation energies in the 1.1−8.0 kcal/mol range. The error in all of the parameters determined is approximately 10%.

The rhombicity of the local potential typically increases as a function of temperature. This is rationalized in terms of two different sources of temperature-dependent structural changes which we identify with persisting proximal restraints, and distal restraints prone to freeze out at lower temperatures. This interpretation is consistent with other studies of HP36.

Previous approaches combined several independent restricted motional modes in a case-specific manner. Typically four quantities, differing in their physical nature, are used as descriptors. MOMD has the benefit of generality, simplicity of the dynamic picture, versatility, within the scope of physical rigor. The SRLS/MOMD/NMR scheme makes possible analyzing internal protein mobility in the liquid and solid states with the same physically appropriate model.

Future prospects include extension to the ^{2}H relaxation limit, application to ^{15}N and ^{13}C, inclusion of collective motions, and accounting for anisotropic (membrane-like) environments. Although we have not considered them in this study, more detailed MOMD analyses, and further comparison with experiment, could include the effects of a nonaxial diffusion tensor, separate ordering and diffusion tensor frames, and additional terms in the expansion of the potential (eq 3). Even without such refinements, useful results were obtained, providing a consistent physical picture.

DOI: 10.1021/jp511386b
J. Phys. Chem. B 2015, 119, 2857−2868

AUTHOR INFORMATION

Corresponding Authors

*E-mail: eva.meirovitch@biu.ac.il. Phone: 972-3-531-8049
*E-mail: jhf3@cornell.edu. Phone: 1-607-255-3647.

Notes

The authors declare no competing financial interest.

ACKNOWLEDGMENTS

This work was supported by the Israel - U.S.A. Binational Science Foundation (Grant No. 2010185 to E.M. and J.H.F.) and the Israel Science Foundation (Grant No. 437/11 to E.M.). This work was also supported by NIH/NIGMS grant P41GM103521 to J.H.F.

REFERENCES

(1) Comellas, G.; Rienstra, C. Protein Structure Determination by Magic-Angle Spinning Solid-State NMR, and Insights into the Formation, Structure and Stability of Amyloid Fibrils. M. *Annu. Rev. Biophys.* **2013**, *42*, 515−536.

(2) Krushelnitsky, A.; Reichert, D.; Saalwachter, K. Solid-state NMR Approaches to Internal Dynamics of Proteins: from Picoseconds to Microseconds and Seconds. *Accnt. Chem. Res.* **2013**, *46*, 2028−2036.

(3) Lewadowski, J. R. Advances in Solid-State Relaxation Methodology for Probing Site-Specific Protein Dynamics. *Acc. Chem. Res.* **2013**, *46*, 2018−2027.

(4) Watt, E. D.; Rienstra, C. M. Recent Advances in Solid-State Nuclear Magnetic Resonance Techniques to Quantify Biomolecular Dynamics. *Anal. Chem. Rev.* **2013**, *86*, 58−64.

(5) Linser, R.; Sarkar, R.; Krushelnitzky, A.; Mainz, A.; Reif, B. Dynamics in the Solid-State: Perspectives for the Investigation of Amyloid Aggregates, Membrane Proteins and Soluble Protein Complexes. *J. Biomol. NMR* **2014**, *59*, 1−14.

(6) Abu-Baker, S.; Lu, J.-X.; Chu, S.; Brinn, C. C.; Makaroff, C. A.; Lorigan, G. A. Side-Chain and Backbone Dynamics of Phospholamban in Phospholipid Bilayers Utilizing ^{2}H and ^{15}N Solid-State NMR Spectroscopy. *Biochemistry* **2007**, *46*, 11695−11706.

(7) Sparks, S. W.; Budhu, N.; Young, P. E.; Torchia, D. A. Side-Chain Dynamics of Crystalline L-[3,3-$^{2}H_2$] Methionine Studied by NMR Spectroscopy. *J. Am. Chem. Soc.* **1988**, *110*, 3359−3367.

(8) Batchelder, L. S.; Sullivan, C. E.; Jelinski, L. W.; Torchia, D. A. Characterization of Leucine Side-Chain Reorientation in Collagen Fibrils by Solid-State ^{2}H NMR. *Proc. Natl. Acad. Sci. U.S.A.* **1982**, *79*, 386.

(9) Keniry, M. A.; Rothgeb, M.; Smith, R. L.; Gutowsky, H. S.; Oldfield, E. Nuclear Magnetic Resonance Studies of Amino Acids and Proteins. Side-Chain Mobility of Methionine in the Crystalline Amino Acid and in Crystalline Sperm Whale (*Physester Catodon*) Myoglobin. *Biochemistry* **1983**, *22*, 1917−1926.

(10) Spiess, H. W. In *Dynamic NMR spectroscopy*; Diehl, P., Fluck, E., Kosfeld, R., Eds.; Springer-Verlag: Berlin, 1978; Vol. *15*, pp 55 - 241.

(11) Wittebort, R. J.; Olejniczak, E. T.; Griffin, R. G. Analysis of Deuterium Nuclear Magnetic Resonance Line Shapes in Anisotropic Media. *J. Chem. Phys.* **1987**, *86*, 5411−5420.

(12) Vold, R. R.; Vold, R. L. Deuterium Relaxation in Molecular Solids. *Adv. Magn. Opt. Reson.* **1991**, *16*, 85−171.

(13) Alam, T. M.; Drobny, G. P. Solid-State NMR Studies of DNA Structure and Dynamics. *Chem. Rev.* **1991**, *91*, 1545−1590.

(14) Campbell, R. F.; Meirovitch, E.; Freed, J. H. Slow Motional NMR Lineshapes of Very Anisotropic Rotational Diffusion: Phosphorus-31 NMR of Phospholipids. *J. Phys. Chem.* **1979**, *83*, 525.

(15) Meirovitch, E.; Freed, J. H. Slow Motional Lineshapes for Very Anisotropic Diffusion: I = 1 Nuclei. *Chem. Phys. Lett.* **1979**, *64*, 311.

(16) Schwartz, L. J.; Meirovitch, E.; Ripmeester, J. A.; Freed, J. H. A Quadrupole Echo Study of Internal Motions in Polycrystalline Media. *J. Phys. Chem.* **1983**, *87*, 4453−4461.

(17) Vugmeyster, L.; Ostrovsky, D.; Ford, J. J.; Burton, S. D.; Lipton, A. S.; Hoatson, G. L.; Vold, R. L. Probing the Dynamics of a Protein Hydrophobic Core by Deuteron Solid-State Nuclear Magnetic Resonance Spectroscopy. *J. Am. Chem. Soc.* **2009**, *131*, 13651−13658.

(18) Vugmeyster, L.; Ostrovsky, D.; Khadjinova, A.; Elleden, J.; Hoatson, G. L.; Vold, R. L. Slow Motions in the Hydrophobic Core of Chicken Villin Headpiece Subdomain and their Contributions to Configurational Entropy and Heat Capacity from Solid-State Deuteron NMR Measurements. *Biochemistry* **2011**, *50*, 10637−10646.

(19) Vugmeyster, L.; Ostrovsky, D.; Penland, K.; Hoatson, G. L.; Vold, R. L. Glassy Dynamics of Protein Methyl Groups Revealed by Deuteron NMR. *J. Phys. Chem. B* **2013**, *117*, 1051−1061.

(20) Vugmeyster, L.; Ostrovsky, D. Restricted Diffusion of Methyl Groups in Proteins Revealed by Deuteron NMR: Manifestation of Intra-Well Dynamics. *J. Chem. Phys.* **2014**, *140*, 075101−10.

(21) Breen, N. F.; Weidner, T.; Li, K.; Castner, D. G.; Drobny, G. P. A Solid-State Deuterium NMR and Sum-Frequency Generation Study of the Side-Chain Dynamics of Peptides Adsorbed onto Surfaces. *J. Am. Chem. Soc.* **2009**, *131*, 14148−14149.

(22) Weidner, T.; Breen, T. F.; Li, K.; Drobny, G. P.; Castner, D. G. Sum Frequency Generation and Solid-State NMR Study of the Structure, Orientation and Dynamics of Polystyrene-Adsorbed Particles. *Proc. Natl. Acad. Sci. U.S.A.* **2010**, *107*, 13288−13293.

(23) Breen, N. F.; Li, K.; Olsen, G. L.; Drobny, G. P. Deuterium Magic Angle Spinning NMR Used to Study the Dynamics of Peptides Adsorbed onto Polystyrene and Functionalized Polystyrene Surfaces. *J. Phys. Chem. B* **2011**, *115*, 9452−9460.

(24) Li, K.; Emani, P. S.; Ash, J.; Groves, M.; Drobny, G. P. A Study of Phenylalanine Side-Chain Dynamics in Surface-Adsorbed Peptides Using Solid-State Deuterium NMR and Rotamer Library Statistics. *J. Am. Chem. Soc.* **2014**, *136*, 11402−11411.

(25) Vold, R. L.; Hoatson, G. L.; Vugmeyster, L.; Ostrovski, D.; De Castro, P. J. Solid-State Deuteron Relaxation Time Anisotropy Measured with Multiple Echo Acquisition. *Phys. Chem. Chem. Phys.* **2009**, *11*, 7008−7012.

(26) Gath, J.; Hoatson, G. L.; Vold, R. L.; Berthoud, R.; Coperet, C.; Grellier, M.; Sabo-Etienne, S.; Lesage, A.; Emsley, L. Motional Heterogeneity in Single-Site Silica-Supported Species Revealed by Deuteron NMR. *Phys. Chem. Chem. Phys.* **2009**, *11*, 6962−6971.

(27) Roehrich, A.; Drobny, G. P. Solid-State NMR Studies of Biomineralization Peptides and Proteins. *Acc. Chem. Res.* **2013**, *46*, 2136−2144.

(28) Maliniak, A.; Greenbaum, S.; Poupko, R.; Zimmermann, H.; Luz, Z. Deuterium and Carbon-13 NMR of Solid and Discotic Phased of Three Benzene Alkanoates. *J. Phys. Chem.* **1993**, *97*, 4832−4840.

(29) Baker, L. A.; Baldus, M. Characterization of Membrane Protein Function by Solid-State NMR Spectroscopy. *Curr. Opin. Struct. Biol.* **2014**, *27C*, 48−55.

(30) Wang, S.; Munro, R. A.; Shi, L.; et al. Solid-State NMR Spectroscopy Structure Determination of a Lipid-Embedded Heptahelical Membrane Protein. *Nat. Methods* **2013**, *10*, 1007−1012.

(31) Copié, V.; McDermott, A. E.; Beshah, K.; Williams, J. C.; Spijker-Assink, M.; Gebhard, R.; Lugtenburg, J.; Herzfeld, J.; Griffin, R. G. Deuterium Solid-State Nuclear Magnetic Resonance Studies of Methyl Group Dynamics in Bacteriorhodopsin and Retinal Model Compounds: Evidence for a 6-s-Trans Chromophore in the Protein. *Biochemistry* **1994**, *33*, 3280−3286.

(32) Ying, W.; Irvine, S. E.; Beekman, R. D.; Smith, S. O.; Simionovitch, D. J. Deuterium NMR Reveals Helix Packing Interactions in Phospholamban. *J. Am. Chem. Soc.* **2000**, *122*, 11125−11128.

(33) Tong, K. I.; Yamamoto, M.; Tanaka, T. Selective Isotope Labeling of Recombinant Proteins in *Escherichia Coli*. *Methods Mol. Biol.* **2012**, *896*, 439−448.

(34) Tugarinov, V.; Kanelis, V.; Kay, L. E. Isotope Labeling Strategies for the Study of High-Molecular-Weight Proteins by Solution NMR Spectroscopy. *Nat. Protoc.* **2006**, *1*, 749−754.

(35) Linser, R.; Gelev, V.; Hagn, F.; Arthanari, H.; Hyberts, S. G.; Wagner, G. Selective Methyl Labeling of Eukaryotic Membrane Proteins Using Cell-Free Expression. *J. Am. Chem. Soc.* **2014**, *136*, 11308−11310.

DOI: 10.1021/jp511386b
J. Phys. Chem. B 2015, 119, 2857−2868

(36) Huang, T. H.; Skarjune, R. P.; Wittebort, R. J.; Griffin, R. G.; Oldfield, E. Restricted Rotational Isomerization in Polymethylene Chains. *J. Am. Chem. Soc.* **1980**, *102*, 7379−7381.
(37) Torchia, D. A.; Szabo, A. Spin-Lattice Relaxation in Solids. *J. Magn. Reson.* **1982**, *49*, 107−121.
(38) Brown, M. F.; Heyn, M. P.; Job, C.; Kim, S.; Moltke, S.; Nakanishi, K.; Nevzorov, A. A.; Struts, A. V.; Salgado, G. F. J.; Wallat, I. Solid-State ^{2}H NMR Spectroscopy of Retinal Proteins in Aligned Membranes. *Biochim. Biophys. Acta* **2007**, *1768*, 2979−3000.
(39) Vold, R. L.; Hoatson, G. L. Effects of Jump Dynamics on Solid State Nuclear Magnetic Resonance Line Shapes and Spin Relaxation Times. *J. Magn. Reson.* **2009**, *198*, 57−72.
(40) Avitabile, J.; London, R. E. Calculated Carbon-13 NMR Relaxation Parameters for a Restricted Internal Diffusion Model. Application to Methionine Relaxation in DHFR. *J. Am. Chem. Soc.* **1978**, *100*, 7159−7165.
(41) Tamura, A.; Matsushita, M.; Naito, A.; Kojima, S.; Miura, K.-I.; Akasaka, K. Dynamics of the Three Methionyl Side Chains of *Streptomyces* Subtilisin Inhibitor. Deuterium NMR Studies in Solution and in the Solid-State. *Protein Sci.* **1996**, *5*, 127−139.
(42) Echodu, D.; Goobes, G.; Shajani, Z.; Pederson, K.; Meints, G.; Varani, G.; Drobny, G. P. Furanose Dynamics in the *Hha*I Methyltransferase Target DNA Studied by Solution and Solid-State NMR Relaxation. *J. Phys. Chem. B* **2008**, *112*, 13934−13944.
(43) Polnaszek, C. F.; Bruno, G. V.; Freed, J. H. ESR Lineshapes in the Slow-Motional Region: Anisotropic Liquids. *J. Chem. Phys.* **1973**, *58*, 3185−3199.
(44) Polnaszek, C. F.; Freed, J. H. Electron Spin Resonance Studies of Anisotropic Ordering, Spin Relaxation, and Slow Tumbling in Liquid Crystalline Solvents. *J. Phys. Chem.* **1975**, *79*, 2283−2306.
(45) Lin, W. J.; Freed, J. H. Electron Spin Resonance Studies of Anisotropic Ordering, Spin Relaxation, and Slow Tumbling in Liquid Crystalline Solvents: 3. Smectics. *J. Phys. Chem.* **1979**, *83*, 379−401.
(46) Schneider, D. J.; Freed, J. H. Spin relaxation and molecular dynamics. In *Lasers, Molecules and Methods*; Hirshfelder, J. O., Wyatt, R. E., Coalson, R. D., Eds.; Adv. Chem. Phys.; John Wiley and Sons: New York, 1989; Vol. *73*, pp 387−528.
(47) Nordio, P. L.; Busolin, P. Electron Spin Resonance Line Shapes in Partially Oriented Systems. *J. Chem. Phys.* **1971**, *55*, 5485.
(48) Misra, S. K.; Freed, J. H. *Multifrequency electron paramagnetic resonance*; Misra, S. K., Ed.; Wiley-VCH: New York, 2011; Vol. *11*, pp 497−544.
(49) Polimeno, A.; Freed, J. H. Slow-Motional ESR in Complex Fluids: the Slowly Relaxing Local Structure Model of Solvent Cage Effects. *J. Phys. Chem.* **1995**, *99*, 10995−11006.
(50) Meirovitch, E.; Nayeem, A.; Freed, J. H. Protein-Lipid Interactions: a Single-Site Interpretation of the ESR Spectra. *J. Phys. Chem.* **1984**, *88*, 3454−3465.
(51) Liang, Z.; Lou, Y.; Freed, J. H.; Columbus, L.; Hubbell, W. L. A Multifrequency Electron Spin Resonance Study of T4 Lysozyme Using the Slowly Relaxing Local Structure Model. *J. Phys. Chem. B* **2004**, *108*, 17649−17659.
(52) Liang, Z.; Freed, J. H.; Keyes, R. S.; Bobst, A. M. An Electron Spin Resonance Study of DNA Dynamics Using the Slowly Relaxing Local Structure Model. *J. Phys. Chem. B* **2000**, *104*, 5372−5381.
(53) Ferrarini, A.; Moro, G. J.; Nordio, P. L. Conformational Kinetics of Aliphatic Tails. *Mol. Phys.* **1988**, *63*, 225.
(54) Moro, G. J. The Coupling Between Librational Motions and Conformational Transitions in Chain Molecules: a Phenomenological Analysis. *J. Chem. Phys.* **1991**, *94*, 8577.
(55) Tombolato, F.; Ferrarini, A.; Freed, J. H. Dynamics of Nitroxide Side Chains in Spin-Labeled Proteins. *J. Phys. Chem. B* **2006**, *110*, 26248−26259.
(56) Heaton, N. J. Simulation of Dynamic NMR Spectral of Rotating Solids. *Mol. Phys.* **1997**, *92*, 251−263.
(57) Meints, G. A.; Karlsson, T.; Drobny, G. P. Solid-State Nuclear Magnetic Resonance Spectroscopy of Furanose Ring Dynamics in the DNA *Hha*I Binding Site. *J. Am. Chem. Soc.* **2001**, *123*, 10030−10038.
(58) Polimeno, A.; Freed, J. H. A Many-Body Stochastic Approach to Rotational Motions in Liquids. *Adv. Chem. Phys.* **1993**, *83*, 89−204.
(59) Liang, Z.; Freed, J. H. An Assessment of the Applicability of Multifrequency ESR to Study the Complex Dynamics of Biomolecules. *J. Phys. Chem. B* **1999**, *103*, 6384−6396.
(60) Tugarinov, V.; Liang, Z.; Shapiro, Yu. E.; Freed, J. H.; Meirovitch, E. A Structural Mode-Coupling Approach to ^{15}N NMR Relaxation in Proteins. *J. Am. Chem. Soc.* **2001**, *123*, 3055−3063.
(61) Meirovitch, E.; Shapiro, Yu. E.; Polimeno, A.; Freed, J. H. Protein Dynamics from NMR: the SRLS Analysis Compared with MF Analysis. *J. Phys. Chem. A* **2006**, *110*, 8366−8396.
(62) Meirovitch, E.; Shapiro, Yu. E.; Polimeno, A.; Freed, J. H. Structural Dynamics of Bio-Macromolecules by NMR: the Slowly Relaxing Local Structure Approach. *Prog. NMR Spectrosc.* **2010**, *56*, 360−405.
(63) Lewandowski, J. R.; Sein, J.; Blackledge, M.; Emsley, L. Anisotropic Collective Motion Contributes to Nuclear Spin Relaxation in Crystalline Proteins. *J. Am. Chem. Soc.* **2009**, *132*, 1246−1248.
(64) Hackel, C.; Zinkevich, T.; Belton, P.; Achilles, A.; Reichert, D.; Krushelnitsky, A. The Trehalose Coating Effect on the Internal Protein Dynamics. *Phys. Chem. Chem. Phys.* **2012**, *14*, 2727−2734.
(65) Shapiro, Yu. E.; Polimeno, A.; Freed, J. H.; Meirovitch, E. Methyl Dynamics of a Ca^{2+}- Calmodulin-Peptide Complex from NMR/SRLS. *J. Phys. Chem. B* **2011**, *115*, 354−365.
(66) Igumenova, T. I.; Frederick, K. K.; Wand, J. A. Characterization of the Fast Dynamics on Protein Amino-Acid Side Chains Using NMR Relaxation in Solution. *Chem. Rev.* **2006**, *106*, 1672−1699.
(67) Shapiro, Yu. E.; Meirovitch, E. Slowly Relaxing Local Structure (SRLS) Analysis of ^{15}N-H Relaxation from the Prototypical Small Proteins GB1 and GB3. *J. Phys. Chem. B* **2012**, *116*, 4056−4068.
(68) Zerbetto, M.; Anderson, R.; Bouguet-Bonnet, S.; Rech, M.; Zhang, L.; Meirovitch, E.; Polimeno, A.; Buck, M. Analysis of ^{15}N−^{1}H NMR Relaxation in Proteins by a Combined Experimental and Molecular Dynamics Simulation Approach. Picosecond-Nanosecond Dynamics of the Rho GTPase Binding Domain of Plexin-B_1 in the Dimeric State Indicates Allosteric Pathways. *J. Phys. Chem. B* **2013**, *117*, 174−184.
(69) Vugmeyster, L.; Trott, O.; McKnight, J.; Raleigh, D. P.; Palmer, A. G. Temperature-Dependent Dynamics of Villin Headpiece Helical Subdomain, an Unusually Small Thermostable Protein. *J. Mol. Biol.* **2002**, *320*, 841−854.
(70) Herges, T.; Wenzel, W. Free-Energy Landscape of the Villin Headpiece in an All-Atom Force-Field. *Structure* **2005**, *13*, 661−668.
(71) Wickstrom, L.; Yuan, B.; Hornak, V.; Raleigh, D. P.; Simmerling, C. Reconciling the Solution and X-Ray Structures of Villin Headpiece Helical Subdomain: Molecular Dynamics and Double-Mutant Cycles Reveal a Stabilizing Cation-π Interaction. *Biochemistry* **2007**, *46*, 3624−3634.
(72) Hassan, S.; Schade, M.; Shaw, C. P.; Levy, R.; Hamm, P. Response of Villin Headpiece-Capped Gold Nanoparticles to Ultrafast Laser Heating. *J. Phys. Chem. B* **2014**, *118*, 7954−7962.

DOI: 10.1021/jp511386b
J. Phys. Chem. B 2015, 119, 2857−2868